Frontiers in Health InformaticsISSN-Online: 2676-7104
www.healthinformaticsjournal.com
2024; Vol 13: Issue 7
Open Access

A Study on Deep Learning Algorithm Conditions for Improving the Accuracy of Carious Tooth Detection in Panoramic Radiographic Images

Hyun-Jun Ahn[1] and Sang-Hyun Kim[2]
[1]Department of Dental Radiology, SMG-SNU Boramae Medical Center, South Korea
[2]Department of Radiological Science, Shin-Han University, South Korea

Cite this paper as:
Hyun-Jun Ahn and Sang-Hyun Kim (2024). A Study on Deep Learning Algorithm Conditions for Improving the Accuracy of Carious Tooth Detection in Panoramic Radiographic Images. *Frontiers in Health Informatics,* 13(7), 1292-1303

ABSTRACT
This study conducted research on an object detection module to distinguish images of carious teeth, a common dental condition, and further sought conditions to support AI in identifying these images more effectively. During the training process using U-Net, 10 process modules were created with the DEEP:PHI program, and training and evaluation were conducted using data augmentation. The Dice and miou values were derived to compare and analyze the accuracy of carious tooth detection based on the degree of area overlap. As a result, the Pre-processing Patch 768×768 module achieved the highest values, with a Dice value of 0.6725 and an miou value of 0.5066. This demonstrates that the use of patch extraction techniques with pre-processing in data augmentation and larger image sizes can improve the accuracy of area segmentation. This study represents an initial attempt to integrate dental panoramic radiographic images with AI, with the expectation that it will serve as a reference for future research. Furthermore, it is anticipated to serve as a foundation for radiologists to apply AI technology to the imaging field, aiming for academic and technological advancements.

Keywords: AI, Panoramic radiography, Caries, Patch extraction, Dice, miou

Ⅰ. INTRODUCTION

Dental caries is one of the most common chronic diseases worldwide, affecting an estimated 30% of the Korean population, who visit dental clinics for treatment of at least one carious lesion on average【1】. This condition involves localized destruction of the tooth structure by microorganisms, resulting in changes to normal structures such as enamel, dentin, and cementum. Radiographically, dental caries can be categorized based on the location of the lesions on the tooth, affecting areas such as the proximal surfaces, occlusal surfaces, buccal surfaces, lingual surfaces, and root surfaces【2】. However, in dental practice, radiographs alone do not enable 100% detection of carious lesions; visual inspection by clinicians is essential. Interpretation challenges arise due to factors like time constraints, examiner skill and experience, and individual variations in tooth structure. To aid in diagnosing the extent and degree of carious lesions, radiographic imaging is frequently used as an adjunct diagnostic tool. Thus, our study aimed to improve diagnostic support using accurate imaging processes【3】.

This study utilized panoramic radiographic images, the most commonly employed basic diagnostic equipment, for their convenience and simplicity. Panoramic radiography is non-invasive and provides comprehensive information on anatomical and pathological features in a single scan【4】. It is particularly valuable in detecting carious lesions across the entire dental structure and supports accurate diagnosis and treatment planning by allowing symmetrical comparisons【5】. However, panoramic radiographic images have limitations in detecting early-stage caries and hidden lesions due to distortion, noise, and subtle changes that are difficult to see with the naked eye【6】. Moreover, interpretive variability necessitates a more precise

and detailed image analysis process to provide objective and accurate lesion information【7】. This study thus focused on advanced image analysis methods, utilizing deep learning techniques from artificial intelligence, which has garnered significant interest with the Fourth Industrial Revolution. We conducted object detection module tasks and explored conditions for training accurate image segmentation to enable AI-assisted image prediction. The use of deep learning technology in this context is expected to improve the efficiency and accuracy of panoramic radiographic images interpretation, potentially serving as a more precise and reliable diagnostic support metric in dentistry.

To provide a clearer understanding of this study, an introduction to dental numbering is included. Each tooth has a unique numbering system to indicate its position. Commonly, the incisors, including the central incisors (tooth 1) and lateral (tooth 2) incisors, are followed by the canine (tooth 3). The premolars, referred to as bicuspids, are numbered as tooth 4 and 5, and the molars, representing the larger posterior teeth, are numbered as teeth 6, 7, and 8, with the third molar (tooth 8) commonly known as the wisdom tooth. Without wisdom teeth, there are typically 28 teeth; including wisdom teeth increases the total count slightly (Fig. 1). In panoramic radiographic images, the left upper quadrant corresponds to the 10 series, the right upper quadrant to the 20 series, the right lower quadrant to the 30 series, and the left lower quadrant to the 40 series (Fig. 2)【8】.

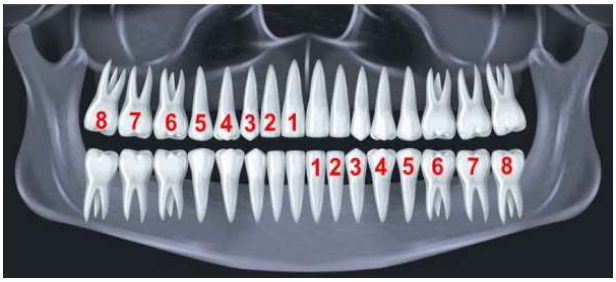

[Fig. 1] Position of the tooth number in anatomy

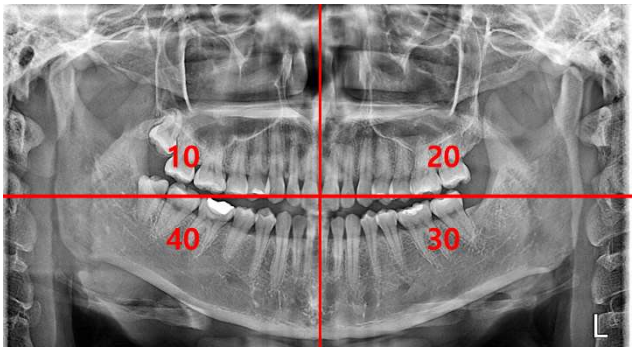

[Fig. 2] Standard for dividing tooth number

Ⅱ. MATERIAL AND METHODS

1. Experimental Equipment and Data Collection

The images used in this study were acquired with the Point 500 CHD panoramic radiography device (Pointnix Co., Gwang-Myeong, Korea) at the dental radiology department of a national university hospital in Seoul. [Fig. 3] The required images were collected from the hospital's INFINITT PACS Software (Infinitt Co., Ltd., Seoul, Korea) for patients seen between January 2022 and August 2024. From the collected images, 90 normal images and 114 caries images were extracted and labeled using the Deep Label program (DEEPNOID Inc., Seoul, Korea). The labeled data were processed through the DEEP:PHI program (DEEPNOID Inc., Seoul, Korea) to create 10 different process modules, enabling training and evaluation through data augmentation.

[Fig. 3] Point 500 CHD

2. AI Model

In this study, we employed U-Net, a model known for its high accuracy in object detection and segmentation, as well as its compatibility with 2D imaging, among the AI models provided by the DEEP:PHI program (DEEPNOID Inc., Seoul, Korea). U-Net is an AI model specialized in segmentation, structured to transform the feature values of input images and convey positional information to the feature values of extracted images through three stages: the contracting path, bottleneck, and expanding path [Fig. 4].

In terms of processing, the contracting path reduces the amount and size of data using max pooling, which extracts data based on the maximum values within each kernel, while doubling the number of channels. In the bottleneck stage, the process transitions from contraction to expansion. In the expanding path, convolution is applied to decrease the amount of data and increase its size, while halving the number of channels.

Medical data often varies in size and frequently comes in high resolution, necessitating careful cropping to appropriately present the data to the AI model. Instead of the sliding window approach—which incrementally scans the image and is computationally intensive and slower—we employed a patch-based extraction method that divides images into a grid without overlap. However, this patch-based approach presents challenges: it reduces the size relative to the input image, resulting in lost segments, and boundary pixels may experience value loss.

Losses resulting from image size reduction were compensated using mirror extrapolation and data augmentation. Mirror extrapolation fills empty spaces by reflecting existing data, creating a mirrored appearance. For data augmentation, an elastic deformation technique was applied, which randomly distorts pixels in various directions.

Losses at boundary pixels were compensated by applying a loss function. This function calculates each pixel's value across the entire image to determine a unique weight for each pixel, then compensates by multiplying the predicted loss value by this unique weight【9】.

$$E=\sum_{x\in\Omega} w(x)\log(P_{\ell(x)}(x))$$

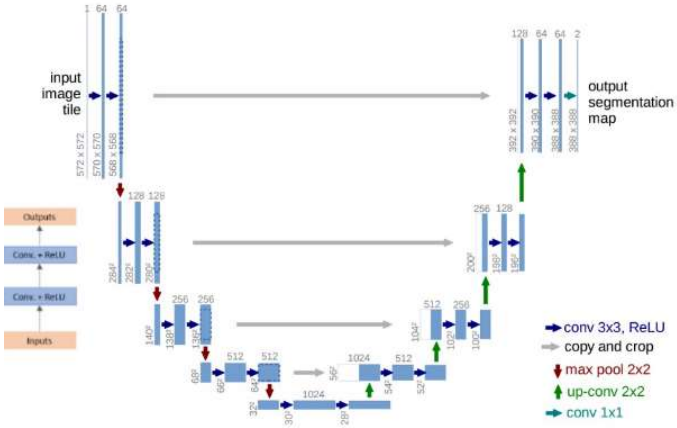

[Fig. 4] Mimetic diagram of U-net

3. RESEARCH METHOD

3.1 Labeling

A total of 204 panoramic dental images were used, including 90 normal images and 114 caries images extracted from the collected data. Labeling of caries regions was performed using the Deep Label program (DEEPNOID Inc., Seoul, Korea). In the program, the Add and Paint functions in the 2D Tools were used to precisely mark the boundaries of caries areas. As shown in Fig. 5, for the panoramic radiographic images, the patient's medical records were referenced to accurately label carious teeth numbered 17, 26, 28, 37, and 46. This labeling process was reviewed with the assistance of one dental radiological technologist, three dental hygienists, and three dental residents, using the patient's medical records as a reference.

To enable caries classification and segmentation by the AI model, 90 normal images and 92 labeled caries images were used as training data, while 11 labeled caries images were used as validation data, and another 11 labeled caries images were used as test data for the final performance evaluation.

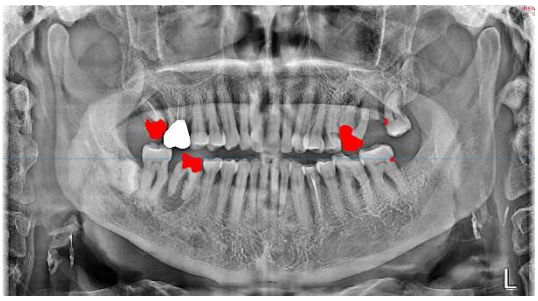

[Fig. 5] Labeling of caries using Deep label program

3.2 Caries Learning Method Using Deep Learning

The previously labeled training data (92 images), validation data (11 images), and test data (11 images) were uploaded to the DEEP:PHI program (DEEPNOID Inc., Seoul, Korea) as an image dataset to prepare for process module creation. Using this dataset, 10 distinct process modules were developed to perform data augmentation for training and evaluation.

The 10 process modules created in this study are as follows:

1) Comparison of data before and after preprocessing

2) Comparison of data based on image size

3) Comparison of data based on Epoch and Batch size

4) Comparison of data according to augmentation techniques

5) Comparison of data based on image shape

6) Comparison of data based on Epoch and Batch size in patch extraction technique

7) Comparison of data based on image size in patch extraction technique

8) Comparison of high-quality data before and after preprocessing in patch extraction technique

9) Comparison of the two best-performing modules

10) Comparison of segmentation results for normal and caries data

This is a schematic of the process modules created within DEEP:PHI. The process module within DEEP:PHI that utilizes preprocessing functions is shown in Fig. 6, while the module that examines the impact of image size by modifying the original images to 256×256, 512×512, and 768×768 is shown in Fig. 7. The module that employs the patch extraction function in DEEP:PHI is illustrated in Fig. 8.

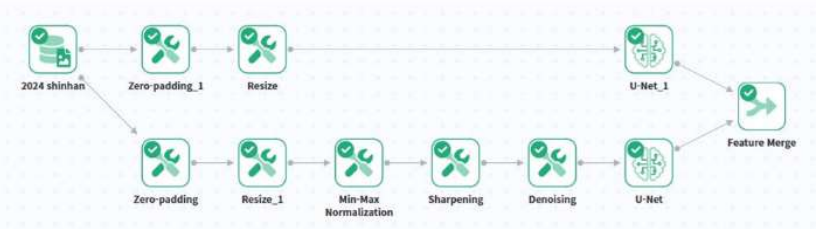

[Fig. 6] Mimetic diagram of DEEP:PHI program module using Pre-processing function

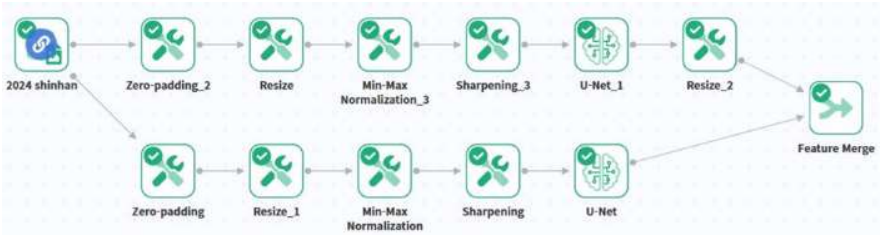

[Fig. 7] Mimetic diagram of DEEP:PHI program module using the Resize function that modify the images size.

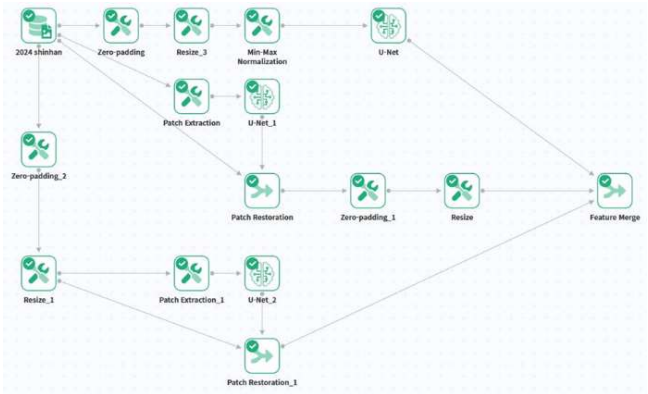

[Fig. 8] Mimetic diagram of DEEP:PHI program module using Patch extraction function.

3.2.1 Training with and without Preprocessing

In this study, five image preprocessing steps were applied. To ensure consistent input and output image sizes for deep learning using convolutional neural networks, zero-padding was applied, maintaining the aspect ratio of the image while resizing it to a 1:1 ratio, converting it to a square shape without distortion. Then, to examine the impact of image size on training accuracy, the original 1500×2615 images were resized to 256×256, 512×512, and 768×768 for training. Next, min-max normalization was used to normalize all pixel values to a range between 0 and 1, ensuring data consistency. The sharpening technique was applied to enhance image edges and highlight important features, while denoising was performed to remove noise, making the images clearer.

3.2.2 Modifying Training Parameters

In this study, we used epoch, batch size, and learning rate decay. The epoch, which determines the number of training iterations, was set to 10, 12, and 120 based on module conditions. Batch size, which represents the number of data samples processed in each iteration, was set to the maximum allowable value for each module, considering the limitations of the Graphics Processing Unit (GPU) resources, and was adjusted according to the epoch value. The learning rate decay was set to 1, allowing the learning rate to decrease with each epoch for faster convergence to optimal results. For fine-tuned optimization, the learning rate was set to 0.0001, with beta_1 and beta_2 values consistently set to 0.9 and 0.999, respectively, across all eight methods, applying the basic Adam optimization approach accordingly.

3.2.3 Learning with Augmentation Techniques

For data augmentation, five scenarios were employed: vertical flip, horizontal flip, rotation, zoom, and crop. All data augmentations were applied randomly and simultaneously within a single loop. The vertical flip involved randomly flipping the images vertically at a certain ratio, where a random number was generated and if it was 0.5 or higher, 50% of the total data was flipped. Similarly, the horizontal flip randomly flipped the images horizontally at a set ratio, again flipping 50% of the total data when the random number was 0.5 or above. The rotation was performed by randomly selecting a rotation angle within a range of ±10°. For the zoom, the images were randomly enlarged within a range of 0.95 to 1.05 times their original size. The crop involved randomly deleting a certain area of the image data within a range of 0 to 0.05%.

3.2.4 Patch Extraction

The patch extraction technique refers to the process of extracting large images into smaller patches. This method divides the images into sections using patch size and stride parameters, employing a grid-like patch search approach without overlap, making it suitable for providing training data for U-Net.

3.3 Segmentation Performance Evaluation Metrics

In this study, to assess the accuracy of caries detection in panoramic radiographic images using deep learning algorithms, we evaluated segmentation accuracy based on the degree of overlap, using Dice and mIoU scores as performance evaluation metrics to validate the model's performance. In calculating these metrics, true positive (TP) represents correctly identified carious teeth, true negative (TN) represents correctly identified healthy teeth, false positive (FP) indicates carious teeth mistakenly identified as healthy, and false negative (FN) indicates healthy teeth mistakenly identified as carious. The formulas for calculating Dice and mIoU scores are provided in equations (1) and (2).

$$Dice\,Coefficient = \frac{2TP}{(TP+FP)+(TP+FN)} \quad (1)$$

$$mIoU = \frac{TP}{TP+FP+FN} \quad (2)$$

The Dice Coefficient measures the similarity between the predicted region and the actual region, indicating the degree of overlap between the two. A value closer to 1 signifies that the prediction aligns more closely with the actual data. The mean Intersection over Union (mIoU) is a metric that measures the ratio of the

intersection to the union of the predicted and actual segmentation areas, averaged across all instances. A value closer to 1 indicates that the model's predictions are more consistent with the actual data.

Ⅲ. RESULT

The comparison of the pre-processing and post-processing data among the ten process modules is presented in Table 1. The results for the pre-processing image, labeled as "without pre-processing," yielded a Dice score of 0.2944 and an mIoU score of 0.1827. In contrast, the post-processing image, labeled as "with pre-processing," produced a Dice score of 0.4973 and an mIoU score of 0.3309. These findings indicate that the post-processed images showed greater similarity to the ground truth images compared to the pre-processed images.

[Table. 1] Segmentation results of without pre-processing data and with pre-processing data.

Data set	Dice	Miou
Without pre-processing	0.2944	0.1827
With pre-processing	0.4973	0.3309

To observe the changes based on image size, the Resize function was applied to set the dimensions to 256×256, 512×512, and 768×768. The results of the segmentation based on image size are shown in Table 2. For the image resized to 256×256, the segmentation yielded a Dice score of 0.2518 and an mIoU score of 0.1440. For the image resized to 512×512, the segmentation produced a Dice score of 0.5768 and an mIoU score of 0.4053. Finally, for the image resized to 768×768, the segmentation resulted in a Dice score of 0.6230 and an mIoU score of 0.4525. These results indicate that larger images with smaller pixel sizes showed greater similarity to the ground truth images.

[Table. 2] Segmentation results according to image size

Data set	Dice	mIoU
Image size 256·256	0.2518	0.1440
Image size 512·512	0.5768	0.4053
Image size 768·768	0.6230	0.4525

The comparison of data based on epoch and batch size is presented in Table 3. When the parameters were set to epoch: 5 and batch size: 4, the results yielded a Dice score of 0.4263 and an mIoU score of 0.2709. In contrast, when the parameters were set to epoch: 10 and batch size: 8, the results showed a Dice score of 0.5768 and an mIoU score of 0.4053. These findings suggest that larger values for the training-related parameters lead to greater similarity with the ground truth images.

[Table. 3] Segmentation results of data before and after increase in epoch and batch size.

Data set	Dice	mIoU
epoch: 5, batch size: 4	0.4263	0.2709
epoch: 10, batch size: 8	0.5768	0.4053

The results comparing the training data augmented by different techniques are presented in Table 4. In the three augmentation conditions using Rotate, Zoom, and Crop, the Dice score was 0.2496 and the mIoU score was 0.1426. In contrast, the five augmentation conditions that included Vertical Flip, Horizontal Flip, Rotate, Zoom, and Crop yielded a Dice score of 0.5768 and an mIoU score of 0.4053. These findings indicate that using a greater variety of augmentation techniques resulted in predictions that were more similar to the ground truth images compared to using fewer techniques.

[Table. 4] Segmentation results of data according to the number of augmentation techniques used.

Data set	Dice	Miou
3 augmentation conditions	0.2496	0.1426
5 augmentation conditions	0.5768	0.4053

The results regarding the use of zero padding during the preprocessing stage to create square images are shown in Table 5. In the case where zero padding was not applied, referred to as Pre-zero Padding, the Dice score was 0.3806 and the mIoU score was 0.2295. In contrast, when zero padding was applied, known as Post-zero Padding, the Dice score improved to 0.5768 and the mIoU score to 0.4053. These findings suggest that utilizing zero padding in the preprocessing stage led to results that were more similar to the ground truth images compared to the case where zero padding was not used.

[Table. 5] Segmentation results of data with and without zero padding

Data set	Dice	mIoU
Pre-zero padding	0.3806	0.2295
Post-zero padding	0.5768	0.4053

The following study utilized the patch extraction technique to train the original images and reported the changes by increasing the epoch and batch size, as shown in Table 6. The results obtained from the original images that underwent patch extraction yielded a Dice score of 0.5745 and an mIoU score of 0.3584. In contrast, when the parameters were increased to an epoch of 12 and a batch size of 9 for the original images, referred to as the "More Parameter" images, the results showed a Dice score of 0.6312 and an mIoU score of 0.1550. This indicates that while increasing the learning parameters improved the Dice score compared to the original images, the mIoU score actually decreased.

[Table. 6] Segmentation results of patch extracted data for the original image and data with increased parameters after patch extraction

Data set	Dice	mIoU
Original image	0.5745	0.3584
More parameter image	0.6312	0.1550

The images processed using the patch extraction technique showed that utilizing the original images resulted in longer training times, limiting the amount of training that could be performed. Therefore, the data were compared based on different image sizes through resizing. Under the baseline condition of Patch size 512×512, the results yielded a Dice score of 0.4561 and an mIoU score of 0.2748. In comparison, for the Patch size 768×768 condition set for size comparison, the results showed a Dice score of 0.6308 and an mIoU score of 0.4607. This indicates that, when using the patch extraction technique, larger image sizes lead to increased Dice and mIoU scores.

Additionally, based on the results in Table 6, adjustments were made to the epoch and batch size parameters, with the results summarized in Table 7. For the More Parameter Patch size 512×512 condition set with an epoch of 120 and a batch size of 4, the results yielded a Dice score of 0.4941 and an mIoU score of 0.3036. In the More Parameter Patch size 768×768 condition, the results showed a Dice score of 0.6182 and an mIoU score of 0.3523.

Although the batch size was reduced to 4 due to research environment constraints, the results increased when the epoch value was increased tenfold, suggesting that larger batch sizes could lead to even better outcomes.

[Table. 7] Segmentation results of data of patch extraction and data with increased parameters after patch extraction for 512·512 images and 768·768 images.

Data set	Dice	mIoU
Patch 512·512	0.4561	0.2748
Patch 768·768	0.6308	0.4607
More parameter Patch 512·512	0.4941	0.3036
More parameter Patch 768·768	0.6182	0.3523

In initial experiments using the patch extraction technique, it was not possible to include a preprocessing step; however, improvements to the module allowed for the addition of preprocessing to the methodology, which subsequently enhanced the results. Therefore, the results of the Patch size 768×768 images—yielding the best outcomes in previous experiments—were further improved by incorporating a preprocessing step. The results are shown in Table 8, with the Pre-processing Patch size 768×768 condition achieving a Dice score of 0.6725 and an mIoU score of 0.5066, marking the highest values obtained in this study.

[Table. 8] Segmentation results of patch extracted data and patch extracted data after pre-processing for 768 · 768.

Data set	Dice	mIoU
Patch 768·768	0.6308	0.4607
Pre-processing patch 768·768	0.6725	0.5066

In this study, normal and abnormal data were compared to assess the accuracy of the predictions, and the results are presented in Table 9. The analysis of the labeled original images in the "Normal vs. Abnormal" condition yielded a Dice score of 0.3115 and an mIoU score of 0.1642. When analyzing the original images after applying the patch extraction technique, in the "Normal vs. Abnormal using Patch Extraction" condition, a Dice score of 0.5661 and an mIoU score of 0.1736 were obtained. While the patch extraction method produced improved results, both outcomes were still somewhat limited.

[Table. 9] Comparing the Segmentation results of Normal and Abnormal data and the Segmentation results of the patch extracted data.

Data set	Dice	Miou
Normal vs Abnormal	0.3115	0.1642
Normal vs Abnormal using patch extraction	0.5661	0.1736

Ⅳ. DISCUSSION

In this study, we aimed to improve the segmentation accuracy of the deep learning algorithm by designing and applying ten different process modules. As seen in Table 8, the Dice coefficient and mIoU values increased as the size of the pre-processed patch extraction images increased, and as we used more augmentation techniques.

The improvements in results under each condition appear to stem from the use of pre-processing, which enhances the consistency of input images and highlights key features. This allows the model to detect the structure of images more accurately, resulting in higher Dice and mIoU values, as demonstrated in Table 1. In particular, the zero-padding function within the pre-processing steps helped preserve information at the boundary areas, reducing the loss of detail around the edges. This method avoided pixel distortion or transformation, enabling the model to process more accurate information and thereby aiding in detection. It is,

therefore, a suitable pre-processing technique for patch extraction methods using U-Net.

The patch extraction technique used in this study produced better results than pre-processing images with multiple techniques, as it presented images to the AI model in a non-overlapping grid format. This method is faster than the sliding window approach, where the entire image is scanned with overlapping regions, as it eliminates image overlap during scanning. However, with patch extraction, the output image size is reduced compared to the input size, and value loss occurs at the grid boundaries. In U-Net, this loss is compensated for by mirror extrapolation and data augmentation, which likely accounts for the improved Dice and mIoU values observed when applying patch extraction.

In Table 2, we observed that the larger the image size, the higher the Dice coefficient and mIoU values. This result is likely due to the fact that larger input images lead to fewer pixel-level changes and distortions in the contracting path, allowing U-Net to more effectively learn key features. Consequently, noise is reduced, and both training speed and performance are improved. Thus, as shown in Table 2, increasing the image size leads to better Dice and mIoU values.

One of the key parameters set in this study was epoch, which, as it increases, allows the model to repeatedly train on the dataset, optimizing parameter adjustments and improving accuracy. Similarly, as batch size increases, the model can process more data at once, enabling more stable and consistent learning. In other words, as epoch and batch size values increase, training stability and accuracy also improve. This enhanced segmentation performance leads to higher Dice and mIoU values, as demonstrated in Table 3.

Additionally, data augmentation effectively expands the dataset, which is especially beneficial in situations where data is limited, such as with medical imaging. This approach improves the model's generalization ability and leads to greater prediction accuracy . Therefore, as shown in Table 4, combining multiple augmentation techniques results in increased Dice and mIoU values

The limitations and constraints of this study are as follows. The panoramic radiographic images used in this study offer the advantages of being non-invasive, quick, and convenient for diagnosis. However, these images face limitations in capturing subtle anatomical differences and often misinterpret shadows created by dental structures as errors. Additionally, due to the nature of the examination, distortion or magnification can vary by region, which makes it challenging to diagnose lesions using only panoramic radiographs.

Furthermore, the number of training samples was insufficient for deep learning, with 90 normal and 114 caries images. Although data augmentation techniques were applied, the amount of data was still limited for effective deep learning model training, reducing the study's accuracy. To improve the accuracy of AI training, the study excluded images of patients with abnormal dental structures, prosthetics, implants, and very small caries. Therefore, in future studies, it will be essential to secure a more diverse and ample dataset to address these issues.

In this study, an approach to improve the accuracy of deep learning model training was explored by using a patch extraction technique, increasing the settings for epoch and batch size. However, as shown in the More parameter image in Table 6, excessive image size or an overly large batch size led to overfitting, resulting in a decrease in the mIoU score. This problem arose from over-training the dataset, with batch size increase identified as a major contributor to overfitting. Therefore, future studies may benefit from addressing this overfitting issue by increasing GPU resources to support larger batch sizes and various settings. Additionally, creating an environment and platform that allows for more diverse research, free from constraints like credit-based systems, is considered essential.

Initially, preprocessing could not be applied in the standard patch extraction method, but after module improvements allowed for preprocessing in the methodology, results significantly improved. This approach yielded the highest values across all parameter settings, indicating that using the patch extraction technique is the most suitable method for effective image discrimination training. In fact, this method outperformed full image size while requiring less processing time, suggesting it as the optimal condition for training images in

this study.

Lastly, an additional study was conducted to classify images in 2D regions rather than segmenting them, aiming to distinguish between normal and carious teeth. However, this approach did not yield satisfactory results. Due to the requirement for labeling in the program, a primary issue emerged with the presence of very small labeled areas in some cases and lesion-labeled data within the images. This likely caused confusion for the AI in making accurate predictions. As a result, unnecessary information may have been learned from the normal images, which likely impeded the AI model's ability to clearly distinguish between healthy and carious teeth. Moreover, reducing errors in the labeled dataset is essential in classification studies, and addressing these challenges may enable future research to develop a platform for more in-depth classification studies capable of distinguishing between normal and abnormal cases.

Furthermore, as AI technology advances and its integration into medical applications grows, this study serves as a pioneering effort to apply deep learning models in dental radiology. Currently, no prior studies have examined the potential for radiologic technologists to utilize deep learning models in dental imaging. By introducing this combination of radiographic imaging and AI, this study may serve as a foundational reference for future research in this field.

Ⅴ. CONCLUSION

This study aimed to train a deep learning algorithm to detect carious teeth using panoramic radiographic images, which are currently used as diagnostic aids in clinical settings. The goal of the research was to improve the accuracy of carious tooth detection by enhancing the deep learning algorithm, thereby exploring its potential as a new diagnostic support tool.

Through the process of training U-Net with panoramic radiographic images via the DEEP:PHI program, the detection accuracy of carious teeth was improved by modifying various conditions. It was confirmed through the Dice and mIoU values that the accuracy of carious tooth detection increased as preprocessing steps (Min-max normalization, Zero padding, Sharpening, Denoising, Resize) were applied, augmentation techniques (Vertical flip, Horizontal flip, Rotate, Zoom, Crop) were used, and learning parameters (Epoch, Batch size) were increased. This confirmed that using a patch extraction method with preprocessing was the most effective approach for accurate image classification. Thus, it was revealed that the accuracy of segmentation varied depending on the conditions for presenting images to the AI model (preprocessing, augmentation techniques, image size and shape modifications), learning conditions (patch extraction, learning parameters), and the combination of these complex conditions.

This study hopes to serve as a starting point for radiologic technologists to utilize AI technology in the field of imaging, aiming for academic and technical advancements.

ACKNOWLEDGEMENT

This work was supported by the National Research Foundation of Korea(NRF) grant funded by the Korea government(MSIT) (NRF-2022R1G1A1004385).

REFERENCE

[1] Ministry of Health and Welfare • Korea Centers for Disease Control and Prevention, Korea Health Statistics, 2015. 2016.

[2] Chang-Seo Park, (2009), Oral and Maxillofacial Radiology, Komoonsa, pp.280-281, 2009.

[3] D Suryani, M N Shoumi and R Wakhidah, “Object detection on dental x-ray images using deep learning method”, 2020.

[4] https://www.pnudh.co.kr/pnudh/board/view.do?cmnx=67&idx=13

[5] Hyun-Jun Ahn, Comparison of Effective Dose using DAP Value between Dental Radiation Examination Dose Calculation Program(ALARA-Dental) and Actual Equipment, 2022.

[6] Bennett T. Amaechi: Emerging technologies for diagnosis of dental caries: The road so far, J. Appl. Phys. VOL 105, 102047-1 – 102047-9, 2009.

[7] Studies of Automatic Dental Cavity Detection System as an Auxiliary Tool for Diagnosis of Dental Caries in Digital X-ray Image, PROGRESS in MEDICAL PHYSICS Vol. 26, No. 1. March, 2015.

[8] Hyun-Jun Ahn, "Setup and usefulness Evaluation of the Ideal Angle of incidence in Dental Intra-Oral Radiography calculated by Cone Beam Computed Tomography", 2024.

[9] Convolutional Networks for Biomedical Image Segmentation, MICCAI, 2015.

[10] Maharana, K.; Mondal, S.; Nemade, B., "The impact of pre- and post-image processing techniques on deep learning frameworks: A comprehensive review for digital pathology image analysis", 2022, 91–99.

[11] Zhi Han, Baichen Liu, "Deep Convolutional Neural Networks with Zero-Padding:Feature Extraction and Learning.", 2023

[12] Adam Tupper, Christian Gagne, "Analyzing Data Augmentation for Medical Images: A Case Study in Ultrasound Images.", 2024